NUCL SCI TECH (2018) 29:154
https://doi.org/10.1007/s41365-018-0501-2

Predictions for production of superheavy nuclei with $Z = 105$–112 in hot fusion reactions

Xiao-Bin Yu[1] · Long Zhu[1] · Zhi-Han Wu[1] · Fan Li[1] · Jun Su[1] · Chen-Chen Guo[1]

Received: 15 April 2018 / Revised: 29 June 2018 / Accepted: 11 July 2018 / Published online: 26 September 2018

Abstract The effects of mass asymmetry on the production of superheavy nuclei (SHN), within the dinuclear system model, are investigated in this study. It is observed that the fusion probability decreases with decreasing mass asymmetry. A total of 192 possible combinations of projectiles from O to Ti and targets with half-lives longer than 30 days for producing SHN ^{264}Db, ^{265}Db, ^{267}Sg, ^{268}Bh, ^{268}Sg, ^{269}Bh, ^{271}Hs, ^{271}Mt, ^{272}Hs, ^{272}Mt, ^{273}Mt, ^{274}Ds, ^{275}Ds, ^{275}Rg, ^{276}Ds, ^{276}Rg, ^{277}Rg, ^{278}Cn, ^{279}Cn, and ^{280}Cn are examined. Further, the optimal combinations and incident energies for synthesizing these nuclei are predicted. Most of the cross sections for production of SHN are larger than 10 pb; therefore, the process can be carried out with the available experimental equipment.

Keywords DNS model · Systematic study · Fusion reaction · Superheavy nuclei · Evaporation residue cross section

This work was supported by the National Natural Science Foundation of China under Grant No. 11605296; the Natural Science Foundation of Guangdong Province, China (Grant No. 2016A030310208); the National Natural Science Foundation of China under Grant Nos. 11875328, 11405278 and 11605270.

✉ Long Zhu
zhulong@mail.sysu.edu.cn

1 Sino-French Institute of Nuclear Engineering and Technology, Sun Yat-sen University, Zhuhai 519082, China

1 Introduction

In recent years, the synthesis of superheavy elements (SHEs) has been developed considerably, both experimentally and theoretically [1–3] and the periodic table of elements has been significantly extended. After the first successful synthesis of element 117 in 2010, all the elements in the seventh row of the periodic table have been discovered by mankind [3–10], which marks a great advancement in man's cognition of the micro-world and a milestone in the evolution of the synthesis of SHEs. At present, efforts are being made to synthesize superheavy nuclei (SHN) experimentally. The elements from 107 to 113 were synthesized at GSI and RIKEN in cold fusion reactions [3–6], and the elements from 114 to 118 were produced at Dubna in hot fusion reactions using a neutron-rich projectile nucleus ^{48}Ca [1, 7–9]. Presently, scientists are interested in the production of SHEs with $Z \geq 119$, which will be a tremendous breakthrough in the field of nuclear physics. However, in the synthesis of SHEs, the cross sections decrease with the increase in the charge number of the nuclei and are close to or even far below the order of pb, which makes the process very difficult.

In addition, the production and measurement of the isotopes of already-known SHEs, which have not yet been synthesized, is important, as they can provide information on the trends of the decay properties along the neutron axis approaching the proposed neutron magic number, including the "island of stability." The synthesis of new SHN can greatly extend the map of the nuclides. According to the theory of nuclear structure [11–13], there is a double magic SHN, the nuclei in the neighborhood of which are relatively stable. In order to accurately locate the "island of stability," more experimental data need to be available;

therefore, the synthesis of more SHN is evidently important. At present, the main method used in the synthesis of SHN is the heavy-ion fusion evaporation reaction; hence, theoretical study of the process is essential for appropriate performance of the experiments [14–27]. Although the ability to predict the production cross sections and incident energies is limited for theoretical models, it is still beneficial to investigate all the possible combinations systematically and predict the favorable ones for producing SHN [28].

In Fig. 1, the blue crosses represent the nuclei that will be investigated in this work. Due to the transition from the cold fusion reactions to hot fusion reactions, the SHN in this region are not synthesized yet. In this study, the effect of mass asymmetry on the fusion probability and cross sections of the reactions ^{26}Mg + ^{248}Cm, ^{36}S + ^{238}U, ^{48}Ca + ^{226}Ra, which lead to the same compound nucleus ^{274}Hs*, is investigated first. In view of the long duration of the experiments and production rate, combinations of stable projectiles and targets with half-lives longer than 30 days are considered to be suitable. All possible combinations of projectiles from O to Ti and targets with half-lives longer than 30 days for producing SHN ^{264}Db, ^{265}Db, ^{267}Sg, ^{268}Bh, ^{268}Sg, ^{269}Bh, ^{271}Hs, ^{271}Mt, ^{272}Hs, ^{272}Mt, ^{273}Mt, ^{274}Ds, ^{275}Ds, ^{275}Rg, ^{276}Ds, ^{276}Rg, ^{277}Rg, ^{278}Cn, ^{279}Cn, and ^{280}Cn are examined, and some optimal combinations and incident energies for synthesizing these nuclei are suggested.

The article is organized as follows: In Sect. 2, a description of the DNS model is given; Sect. 3 details an analysis of the results of calculation and a prediction of the optimal combinations for synthesizing several SHN in the gap region; Sect. 4 presents the summary and the prospects.

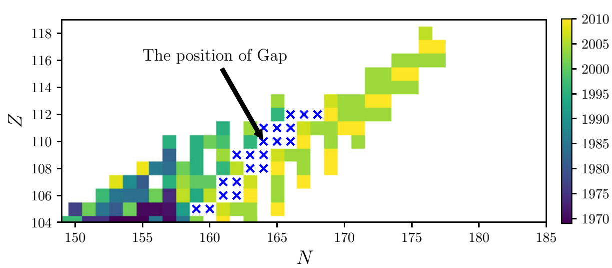

Fig. 1 (Color online) The nuclides in the superheavy area with Z = 105–118. The blue crosses represent the nuclei that will be investigated in this study

2 Theoretical description

According to the concept of the DNS model, the complete fusion reaction is described as a diffusion process. All the nucleons of the projectile are transferred to the target and form a compound nucleus. This process is accompanied by the dissipation of energy and angular momentum. The evaporation residue (ER) cross section of the superheavy nucleus under the incident energy $E_{\mathrm{c.m.}}$ in the center-of-mass frame can be written as [21, 24, 29–34]:

$$\sigma_{\mathrm{ER}}(E_{\mathrm{c.m.}}) = \frac{\pi\hbar^2}{2\mu E_{\mathrm{c.m.}}}\sum_{J=0}^{\infty}(2J+1)T(E_{\mathrm{c.m.}},J) \\ P_{\mathrm{CN}}(E_{\mathrm{c.m.}},J)W_{\mathrm{sur}}(E_{\mathrm{c.m.}},J), \tag{1}$$

where $T(E_{\mathrm{c.m.}}, J)$ is the probability that the collision system overcomes the Coulomb barrier and forms the dinuclear system [35]. $P_{\mathrm{CN}}(E_{\mathrm{c.m.}}, J)$ is the fusion probability. $W_{\mathrm{sur}}(E_{\mathrm{c.m.}}, J)$ is the survival probability of the compound nucleus.

The fusion process described as a diffusion process can be understood by numerically solving the master equations. The time evolution of the distribution probability function $P(Z_1, N_1, t)$ for fragment 1 with the mass number A_1 and excitation energy E_1 at time t is described by the following master equations [17, 24]:

$$\begin{aligned}\frac{\mathrm{d}P(Z_1,N_1,t)}{\mathrm{d}t} &= \sum_{Z_1'} W_{Z_1,N_1;Z_1',N_1}(t)[d_{Z_1,N_1}P(Z_1',N_1,t) \\ &- d_{Z_1',N_1}P(Z_1,N_1,t)] \\ &+ \sum_{N_1'} W_{Z_1,N_1;Z_1,N_1'}(t)[d_{Z_1,N_1}P(Z_1,N_1',t) \\ &- d_{Z_1,N_1'}P(Z_1,N_1,t)] \\ &- [\Lambda^{\mathrm{qf}}_{Z_1,N_1,E_1,t}(\Theta) + \Lambda^{\mathrm{fis}}_{Z_1,N_1,E_1,t}(\Theta)]P(Z_1,N_1,t).\end{aligned} \tag{2}$$

The potential energy surface (PES) of the DNS in the fusion process is defined as:

$$\begin{aligned}U(Z_1,N_1;Z_2,N_2,R) &= E_{\mathrm{B}}(Z_1,N_1) + E_{\mathrm{B}}(Z_2,N_2) \\ &- E_{\mathrm{B}}(Z,N) + V_{\mathrm{C}}(R) + V_{\mathrm{N}}(R),\end{aligned} \tag{3}$$

where $Z = Z_1 + Z_2$ and $N = N_1 + N_2$. $E_{\mathrm{B}}(Z_i, N_i)$ and $E_{\mathrm{B}}(Z, N)$ are the binding energies of the fragment i and the compound nucleus, respectively. V_{C} and V_{N} are the Coulomb potential and nuclear potential, respectively [24].

After the capture process, the DNS is formed. For the formation of the compound nucleus (CN), the projectile should overcome the inner fusion barrier B_{fus}, defined as the difference between U_{BG}, the highest point called Businaro–Gallone (B.G.) point on the left of $U(\eta)$, and the potential at the entrance. Hence, summing up the probability on the left side of the B.G. point, the fusion probability of the DNS is given by [17, 28, 36],

$$P_{\rm CN}(J) = \sum_{Z_1=1}^{Z_{\rm BG}} \sum_{N_1=1}^{N_{\rm BG}} P(Z_1, N_1, E_1(J), \tau_{\rm int}(J)) \ . \tag{4}$$

The compound nucleus formed in the fusion reaction is unstable because of its high excitation energy and usually cools down by emitting γ-rays, evaporating particles (neutrons, protons, α and other light charged particles) and fission [37–39]. This process is described by a statistical model. Subsequent to the fission of the composite nucleus, the survival probability of the SHN after evaporation of x neutrons (considering only neutron evaporation and fission) can be written as:

$$W_{\rm sur}(E^*_{\rm CN}, x, J) = P(E^*_{\rm CN}, x, J) \times \prod_{i=1}^{x} \left[\frac{\Gamma_{\rm n}(E^*_i, J)}{\Gamma_{\rm n}(E^*_i, J) + \Gamma_{\rm f}(E^*_i, J)} \right], \tag{5}$$

where J and $E^*{}_{\rm CN}$ are the spin and excitation energies of the compound nucleus, respectively. The relationship between the excitation energy and incident energy in the center-of-mass frame is $E^*_{\rm CN} = E_{\rm c.m.} + Q$. The nuclear ground state masses are taken from [40]. $\Gamma_{\rm n}(E^*_i, J)$ and $\Gamma_{\rm f}(E^*_i, J)$ are the widths of the ith neutron evaporation and fission, respectively. The solution is described later. E^*_i is the excitation energy of the compound nucleus before evaporation of the ith neutron, which satisfies the following relation: $E^*_{i+1} = E^*_i - B_i n - 2T_i$. $B_i n$ is the evaporation energy of the ith neutron. T_i is the temperature before evaporation of the ith neutron, given by the relation $E^*_i = aT_i 2 - T_i$. The realization probability for neutron evaporation $P(E_{\rm CN}{}^*, x, J)$ can be obtained from Ref. [34].

According to Weisskopf's theory of evaporation, the evaporation width of the particle ν can be written as [41]:

$$\Gamma_\nu(E^*, J) = \frac{(2s_\nu + 1)m_\nu}{\pi^2 \hbar^2 \rho(E^*, J)} \times \int_{I_\nu} \varepsilon \rho(E^* - B_\nu - \varepsilon, J) \sigma_{\rm inv}(\varepsilon) \, {\rm d}\varepsilon, \tag{6}$$

where s_ν is the spin, m_ν is the reduced mass relative to the remaining nucleus, and B_ν is the binding energy, of the evaporating particle ν. $I_\nu = [0, E^* - B_\nu - \delta - \frac{1}{a}]$. The mass table is obtained from Ref. [40]. $\delta = 0, \Delta, 2\Delta$ for odd–odd, odd–even, and even–even nuclei, $\Delta = 11/\sqrt{A}$ MeV. $\sigma_{\rm inv}$ is the inverse reaction cross section for a particle ν with channel energy ε [42]. For the neutron, it is given by $\sigma_{\rm inv} = \pi R^2_\nu$. $R_\nu = 1.16[\sqrt[3]{A - 1} + 1]$.

The width of fission is given by the Bohr-Wheeler formula [43]:

$$\Gamma_{\rm f}(E^*, J) = \frac{1}{2\pi \rho_{\rm f}(E^*, J)} \times \int_{I_{\rm f}} \frac{\rho_{\rm f}(E^* - B_{\rm f} - \varepsilon, J) {\rm d}\varepsilon}{1 + \exp[-2\pi(E^* - B_{\rm f} - \varepsilon)/\hbar\omega]}. \tag{7}$$

Here $I_{\rm f} = [0, E^* - B_{\rm f} - \delta - \frac{1}{a_{\rm f}}]$. $B_{\rm f}(E^*, J)$ is the fission barrier, which is of the form

$$B_{\rm f}(E^*, J) = B^{\rm M}_{\rm f}(E^* = 0, J) \exp\left(-\frac{E^*}{E_{\rm D}} \right). \tag{8}$$

Here, $E_{\rm D} = 20$ MeV is the shell damping energy. $B^{\rm M}_{\rm f}$ is the shell correction energy which is taken from Ref. [40]. After obtaining the widths of neutron evaporation and fission, the final $W_{\rm sur}$ can be obtained from Eq. (5).

3 Results and discussion

In order to investigate qualitatively the effects of mass asymmetry on the fusion probability, the driving potential, which is the minimum value of PES for combinations with the same mass asymmetry, is shown in Fig. 2, as a function of mass asymmetry for the reactions ^{26}Mg + ^{248}Cm, ^{36}S + ^{238}U, and ^{48}Ca + ^{226}Ra, leading to the same compound nucleus ^{274}Hs*. Although the systems evolve in both the proton and neutron degrees of freedom, the mass asymmetry can still be a good collective degree for estimating the fusion probability. The B.G. point is shown in this figure. The blue arrow indicates the inner fusion barrier $B_{\rm fus}$ for the reaction ^{48}Ca + ^{226}Ra. The inner fusion barrier plays a main role in the competition between quasifission and complete fusion. According to the results of the calculation, the inner fusion barriers for the reactions

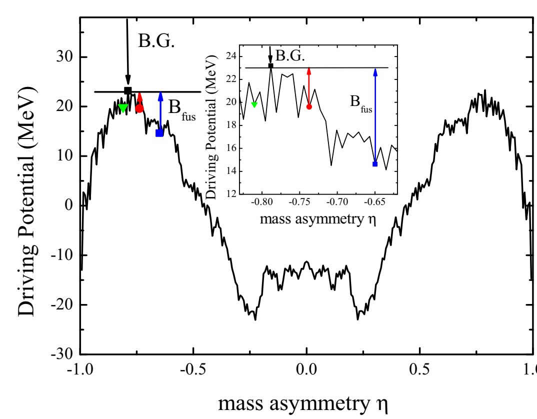

Fig. 2 (Color online) The driving potential of ^{274}Hs* presented as a function of mass asymmetry. The black arrow indicates the B.G. point. The injection points for the reactions ^{26}Mg + ^{248}Cm, ^{36}S + ^{238}U, and ^{48}Ca + ^{226}Ra are denoted by a triangle, solid circle, and square, respectively

$^{36}S + ^{238}U$ and $^{48}Ca + ^{226}Ra$ are $B_{fus,S} = 3.6$ MeV and $B_{fus,Ca} = 8.6$ MeV, respectively. It is observed that the injection point of the reaction $^{26}Mg + ^{248}Cm$ is located on the left side of the B.G. point, therefore, the fusion probability for $^{26}Mg + ^{248}Cm$ would be much larger than that of the other two reactions.

Figure 3 presents the fusion probabilities as a function of the excitation energy of the compound nucleus in the reactions $^{26}Mg + ^{248}Cm$, $^{36}S + ^{238}U$, and $^{48}Ca + ^{226}Ra$. It can be seen from the calculated results that with the same excitation energy, the fusion probability decreases with decreasing mass asymmetry. This is because a near symmetric system can overcome a high inner fusion barrier for forming a compound nucleus by nucleon transfer. The fusion probability for the reaction $^{26}Mg + ^{248}Cm$, is close to 1 and much larger than that of the other two reactions. It can also be seen that the fusion probabilities for all the reactions increase with increasing energy.

Figure 4 shows the excitation functions for the reactions $^{26}Mg + ^{248}Cm$, $^{36}S + ^{238}U$, and $^{48}Ca + ^{226}Ra$. The available experimental data [44–46], which are indicated by points, are also shown. The curves show the results of calculation for different evaporation channels. It can be seen that the calculations duly authenticate the experimental data.

The excitation functions for the reactions $^{22}Ne + ^{254}Cf$, $^{26}Mg + ^{250}Cm$, and $^{48}Ca + ^{228}Ra$ are shown in Fig. 5. All the reactions lead to the same compound nucleus, $^{276}Hs^*$. It can be seen that the cross sections decrease with decreasing mass asymmetry.

However, it cannot be presumed that the reaction with larger value of mass asymmetry is better for producing SHN. For systems with larger values of mass asymmetry, the reactions are usually very hot. Therefore, in the de-excitation process, many neutrons evaporate. This actually limits the neutron richness of the synthesized SHN.

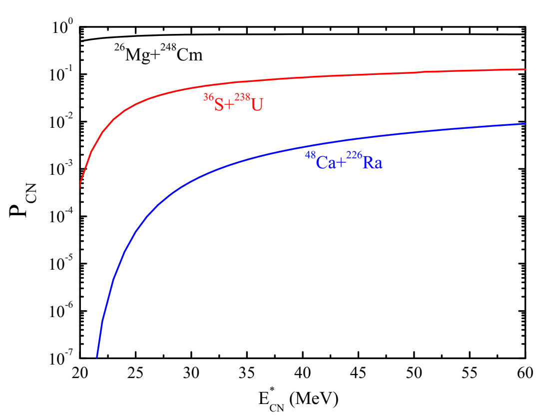

Fig. 3 (Color online) The fusion probability for reactions $^{26}Mg + ^{248}Cm$, $^{36}S + ^{238}U$, and $^{48}Ca + ^{226}Ra$

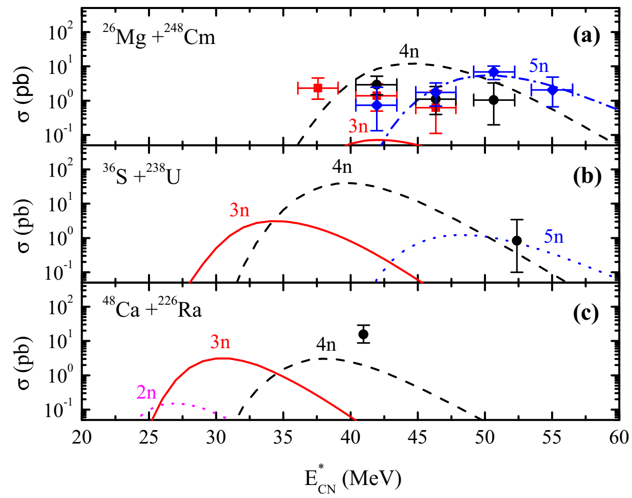

Fig. 4 (Color online) The excitation functions for the reactions $^{26}Mg + ^{248}Cm$ (**a**), $^{36}S + ^{238}U$ (**b**), and $^{48}Ca + ^{226}Ra$ (**c**). The purple dotted lines, red solid lines, black dashed lines, and blue dash-dotted lines represent 2n, 3n, 4n, and 5n evaporation channels, respectively. The red squares, black circles, and blue diamonds represent the experimental data of 3n, 4n, and 5n evaporation channels, respectively [44–46]

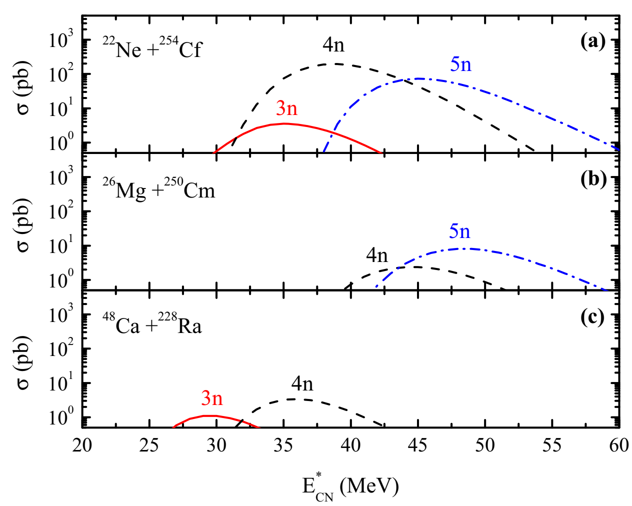

Fig. 5 (Color online) The excitation functions for the reactions $^{22}Ne + ^{254}Cf$ (**a**), $^{26}Mg + ^{250}Cm$ (**b**), and $^{48}Ca + ^{228}Ra$ (**c**)

Moreover, due to the limitation of the target, the projectile cannot be very light. In addition, the mass asymmetry not only affects the fusion probability, but also has an impact on the probability of the capture and survival stages. Therefore, in this study, all the possible combinations are examined systematically, with stable projectiles of $Z = 8$–22 and targets with half-lives longer than 30 days, for synthesizing the unknown SHN, as shown in Fig. 1.

The cross sections of different projectile–target combinations are compared to obtain the optimal ones for synthesizing the unknown SHN, as shown in Figs. 6, 7, 8, 9 and 10. It can be seen that for producing most of these

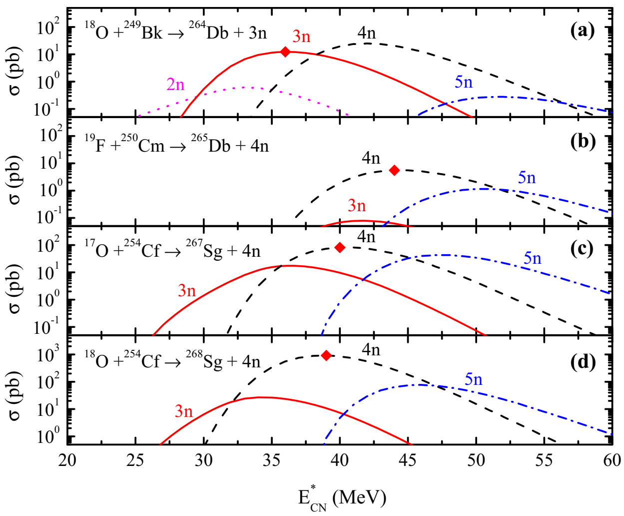

Fig. 6 (Color online) The excitation functions for synthesizing ^{264}Db (**a**), ^{265}Db (**b**), ^{267}Sg (**c**), and ^{268}Sg (d). The purple dotted lines, red solid lines, black dashed lines, and blue dash-dotted lines represent the 2n, 3n, 4n, and 5n evaporation channels, respectively. The red squares, black circles, and blue diamonds represent the experimental data of the 3n, 4n, and 5n evaporation channels, respectively. The red diamonds represent the largest cross sections

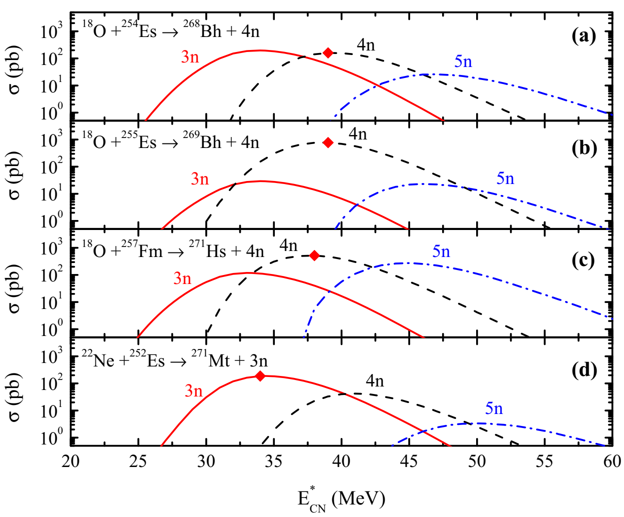

Fig. 7 (Color online) The same as Fig. 6, but for ^{268}Bh, ^{269}Bh, ^{271}Hs, and ^{271}Mt

nuclei, the maximal ER cross sections are larger than 10 pb. For example, for producing the ^{268}Sg, the ER cross section is close to 1 nb in the reaction $^{18}O + ^{254}Es \rightarrow ^{268}Sg + 4n$ with an incident energy of 82.87 MeV. Moreover, for producing the ^{264}Db, ^{265}Db, ^{267}Sg, ^{268}Bh, ^{269}Bh, ^{271}Hs, ^{271}Mt, ^{272}Hs, ^{272}Mt, ^{273}Mt, ^{274}Ds, ^{275}Rg, ^{275}Ds, ^{276}Ds, ^{276}Rg, ^{277}Rg, the most promising reactions are $^{18}O + ^{249}Bk \rightarrow ^{264}Db + 3n$ (12 pb at 79.36 MeV), $^{19}F + ^{250}Cm \rightarrow ^{265}Db + 4n$ (5.6 pb at 89.55 MeV),

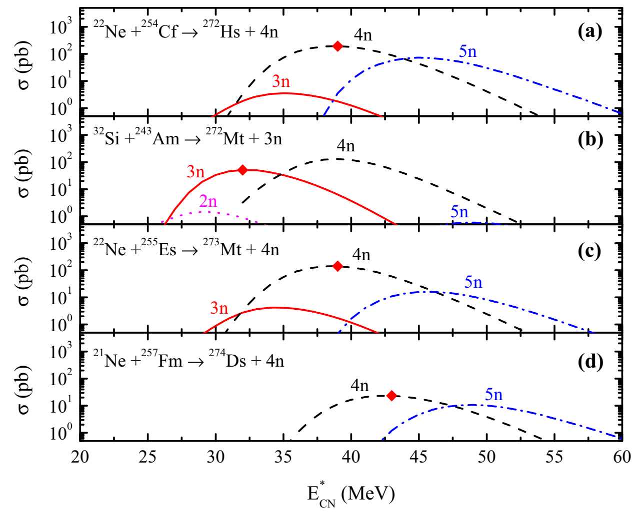

Fig. 8 (Color online) The same as Fig. 6, but for ^{272}Hs, ^{272}Mt, ^{273}Mt, and ^{274}Ds

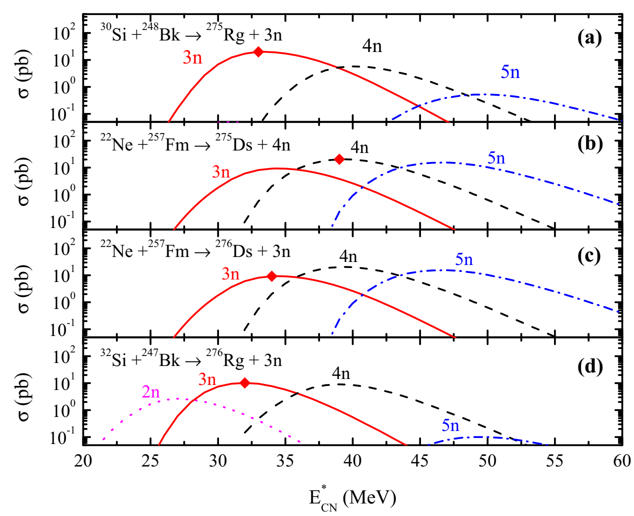

Fig. 9 (Color online) The same as Fig. 6, but for ^{275}Rg, ^{275}Ds, ^{276}Ds, and ^{276}Rg

$^{17}O + ^{254}Cf \rightarrow ^{267}Sg + 4n$ (82 pb at 82.01 MeV), $^{18}O + ^{254}Es \rightarrow ^{268}Bh + 4n$ (160 pb at 84.22 MeV), $^{18}O + ^{255}Es \rightarrow ^{269}Bh + 4n$ (770 pb at 84 MeV), $^{18}O + ^{257}Fm \rightarrow ^{271}Hs + 4n$ (520 pb at 84.56 MeV), $^{22}Ne + ^{252}Es \rightarrow ^{271}Mt + 3n$ (190 pb at 99.25 MeV), $^{22}Ne + ^{254}Cf \rightarrow ^{272}Hs + 4n$ (190 pb at 101.87 MeV), $^{32}Si + ^{243}Am \rightarrow ^{272}Mt + 3n$ (51 pb at 134.9 MeV), $^{22}Ne + ^{255}Es \rightarrow ^{273}Mt + 4n$ (140 pb at 103.52 MeV), $^{21}Ne + ^{257}Fm \rightarrow ^{274}Ds + 4n$ (23 pb at 104.13 MeV), $^{30}Si + ^{248}Bk \rightarrow ^{275}Rg + 3n$ (20 pb at 137.64 MeV), $^{22}Ne + ^{257}Fm \rightarrow ^{275}Ds + 4n$ (20 pb at 104.92 MeV), $^{22}Ne + ^{257}Fm \rightarrow ^{276}Ds + 3n$ (9.2 pb at 99.92 MeV), $^{32}Si + ^{247}Bk \rightarrow ^{276}Rg + 3n$ (10 pb at 139.94 MeV), and $^{32}Si + ^{248}Bk \rightarrow ^{277}Rg + 3n$ (18 pb at 139.31 MeV),

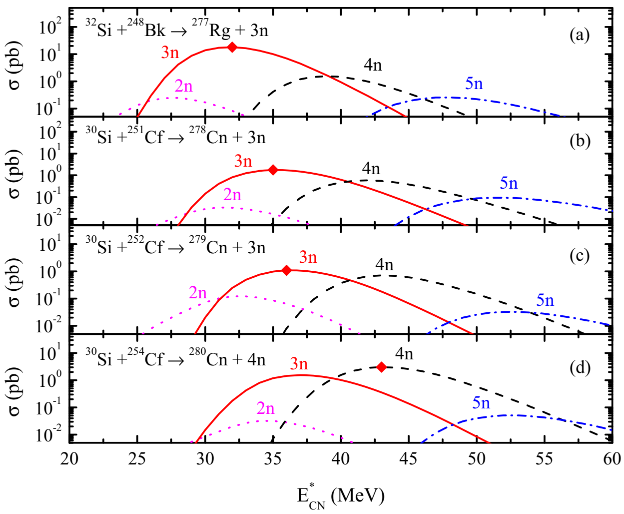

Fig. 10 (Color online) The same as Fig. 6, but for ^{277}Rg, ^{278}Cn, ^{279}Cn, and ^{280}Cn

respectively. However, it can be seen that for synthesis of $^{278-280}$Cn the ER cross sections are approximately 1 pb; therefore, the reaction is still feasible with the available experimental equipment. The maximal evaporation cross sections, optimal incident energies, and corresponding evaporation channels are deduced and presented clearly in Table 1. It is found that for synthesizing the isotopes ^{267}Sg and ^{268}Sg, the target ^{254}Cf can be used. The ^{18}O is predicted as a projectile, for producing both the isotopes ^{268}Bh and ^{269}Bh. In addition, the combinations of projectile and target are the same for synthesizing the ^{275}Ds and ^{276}Ds, but in different evaporation channels.

4 Summary

The production of several SHN was investigated systematically within the dinuclear system model. The mass asymmetry effects were studied, and it was observed that the fusion probabilities decreased with decreasing mass asymmetry. Suitable reactions for producing SHN in the gap region, as shown in Fig. 1, were predicted by reviewing the stable beam-induced hot fusion reactions, and 192 possible combinations with projectiles from O to Ti and targets with half-lives longer than 30 days, for producing SHN ^{264}Db, ^{265}Db, ^{267}Sg, ^{268}Bh, ^{268}Sg, ^{269}Bh, ^{271}Hs, ^{271}Mt, ^{272}Hs, ^{272}Mt, ^{273}Mt, ^{274}Ds, ^{275}Ds, ^{275}Rg, ^{276}Ds, ^{276}Rg, ^{277}Rg, ^{278}Cn, ^{279}Cn, and ^{280}Cn were examined. The optimal combinations and incident energies for synthesizing these nuclei were predicted. It was found that the production cross sections, for synthesizing most of these SHN, were larger than 10 pb. The predicted cross section was 920 pb for the production of ^{268}Sg; hence, the

Table 1 The optimal combinations for synthesis of SHN in the gap

ON	BC	EC	$E_{CN}{}^*$ ($E_{c.m.}$)	$\sigma_{ER,max}$(pb)
^{264}Db	^{18}O + ^{249}Bk	3n	36 (79.36)	1.2×10^1
^{265}Db	^{19}F + ^{250}Cm	4n	44 (89.55)	5.6
^{267}Sg	^{17}O + ^{254}Cf	4n	40 (82.01)	8.2×10^1
^{268}Sg	^{18}O + ^{254}Cf	4n	39 (82.87)	9.2×10^2
^{268}Bh	^{18}O + ^{254}Es	4n	39 (84.22)	1.6×10^2
^{269}Bh	^{18}O + ^{255}Es	4n	39 (84.00)	7.7×10^2
^{271}Hs	^{18}O + ^{257}Fm	4n	38 (84.56)	5.2×10^2
^{271}Mt	^{22}Ne + ^{252}Es	3n	34 (99.25)	1.9×10^2
^{272}Hs	^{22}Ne + ^{254}Cf	4n	39 (101.87)	1.9×10^2
^{272}Mt	^{32}Si + ^{243}Am	3n	32 (134.9)	5.1×10^1
^{273}Mt	^{22}Ne + ^{255}Es	4n	39 (103.52)	1.4×10^2
^{274}Ds	^{21}Ne + ^{257}Fm	4n	43 (104.13)	2.3×10^1
^{275}Rg	^{30}Si + ^{248}Bk	3n	33 (137.64)	2.0×10^1
^{275}Ds	^{22}Ne + ^{257}Fm	4n	39 (104.92)	2.0×10^1
^{276}Ds	^{22}Ne + ^{257}Fm	3n	34 (99.92)	9.2
^{276}Rg	^{32}Si + ^{247}Bk	3n	32 (139.94)	1.0×10^1
^{277}Rg	^{32}Si + ^{248}Bk	3n	32 (139.31)	1.8×10^1
^{278}Cn	^{30}Si + ^{251}Cf	3n	35 (140.57)	1.7
^{279}Cn	^{30}Si + ^{252}Cf	3n	36 (140.22)	1.1
^{280}Cn	^{30}Si + ^{254}Cf	4n	43 (144.86)	3.0

$E_{CN}{}^*$ is the excitation energy where the largest ER cross section appears in the unit of MeV, $E^*_{c.m.}$ is the incident energy in the center-of-mass frame corresponding to $E_{CN}{}^*$

$\sigma_{ER,max}$ is the largest ER cross section in the unit of pb

ON objective nucleus; *BC* best projectile and target combination; *EC* evaporation channel

reaction could be carried out with the available experimental equipment. In future, it would be necessary to carry out systematic calculations on the production of SHN within other theoretical models so that a comparison of the predicted favorable reactions among the different models can provide valuable information regarding the experimental procedure.

References

1. Y.T. Oganessian, V.K. Utyonkov, Superheavy nuclei from ^{48}Ca-induced reactions. Nucl. Phys. A **944**, 62 (2015). https://doi.org/10.1016/j.nuclphysa.2015.07.003

2. V.I. Zagrebaev, W. Greiner, Cross sections for the production of superheavy nuclei. Nucl. Phys. A **944**, 257 (2015). https://doi.org/10.1016/j.nuclphysa.2015.02.010
3. S. Hofmann, G. Münzenberg, The discovery of the heaviest elements. Rev. Mod. Phys. **72**, 733 (2000). https://doi.org/10.1103/revmodphys.72.733
4. S. Hofmann, D. Ackermann, S. Antalic et al., The reaction $^{48}Ca + ^{238}U \rightarrow ^{286}112^*$ studied at the GSI-SHIP. Eur. Phys. J. A **32**, 251 (2007). https://doi.org/10.1140/epja/i2007-10373-x
5. K. Morita, K. Morimoto, D. Kaji et al., New result in the production and decay of an isotope,$^{278}113$, of the 113th element. J. Phys. Soc. Jpn. **81**, 103201 (2012). https://doi.org/10.1143/jpsj.81.103201
6. S. Hofmann, S. Heinz, R. Mann et al., Review of even element super-heavy nuclei and search for element 120. Eur. Phys. J. A **52** (2016). https://doi.org/10.1140/epja/i2016-16180-4
7. Y.T. Oganessian, A.V. Yeremin, A.G. Popeko et al., Synthesis of nuclei of the superheavy element 114 in reactions induced by ^{48}Ca. Nature **400**, 242 (1999a). https://doi.org/10.1038/22281
8. Y.T. Oganessian, V.K. Utyonkov, Y.V. Lobanov et al., Synthesis of superheavy nuclei in the $^{48}Ca+^{244}Pu$ reaction. Phys. Rev. Lett. **83**, 3154 (1999b). https://doi.org/10.1103/physrevlett.83.3154
9. Y.T. Oganessian, F.S. Abdullin, P.D. Bailey et al., Synthesis of a new element with atomic number $Z = 117$. Phys. Rev. Lett. **104**, 142502 (2010). https://doi.org/10.1103/PhysRevLett.104.142502
10. Y. Oganessian, Nuclei in the "Island of Stability" of superheavy elements. J. Phys. Conf. Ser. **337**, 012005 (2012). https://doi.org/10.1088/1742-6596/337/1/012005
11. U. Mosel, W. Greiner, On the stability of superheavy nuclei against fission. Z. Phys. A **222**, 261 (1969). https://doi.org/10.1007/bf01392125
12. S. Nilsson, J. Nix, A. Sobiczewski et al., On the spontaneous fission of nuclei with Z near 114 and N near 184. and P. Möller. Nucl. Phys. A **115**, 545 (1968). https://doi.org/10.1016/0375-9474(68)90748-3
13. P. Moller, J.R. Nix, Stability of heavy and superheavy elements. J. Phys. G Nucl. Part. Phys. **20**, 1681 (1994). https://doi.org/10.1088/0954-3899/20/11/003
14. N. Wang, E.G. Zhao, W. Scheid et al., Theoretical study of the synthesis of superheavy nuclei with $Z = 119$ and 120 in heavy-ion reactions with trans-uranium targets. Phys. Rev. C **85**, 041601 (2012). https://doi.org/10.1103/PhysRevC.85.041601
15. X.J. Bao, S.Q. Guo, H.F. Zhang et al., Influence of proton shell closure on the evaporation residue cross sections of superheavy nuclei. J. Phys. G Nucl. Part. Phys. **44**, 045105 (2017a). https://doi.org/10.1088/1361-6471/aa53e8
16. X.J. Bao, Y. Gao, J.Q. Li et al., Possibilities for synthesis of new isotopes of superheavy nuclei in cold fusion reactions. Phys. Rev. C **93**, 044615 (2016b). https://doi.org/10.1103/PhysRevC.93.044615
17. Z.Q. Feng, G.M. Jin, J.Q. Li, Production of new superheavy $Z = 108 - 114$ nuclei with ^{238}U, ^{244}Pu, and $^{248,250}Cm$ targets. Phys. Rev. C **80**, 057601 (2009a). https://doi.org/10.1103/PhysRevC.80.057601
18. X.J. Bao, S.Q. Guo, H.F. Zhang et al., Influence of entrance channel on production cross sections of superheavy nuclei. Phys. Rev. C **96**, 024610 (2017b). https://doi.org/10.1103/PhysRevC.96.024610
19. M. Huang, Z. Gan, X. Zhou et al., Competing fusion and quasifission reaction mechanisms in the production of superheavy nuclei. Phys. Rev. C **82**, 044614 (2010). https://doi.org/10.1103/PhysRevC.82.044614
20. Z.H. Liu, J.D. Bao, Neutron emission in the fusion process and its effect on the formation of superheavy nuclei. Phys. Rev. C **89**, 024604 (2014). https://doi.org/10.1103/PhysRevC.89.024604
21. Z.H. Liu, J.D. Bao, Q-value effects on the production of superheavy nuclei. Phys. Rev. C **74**, 057602 (2006). https://doi.org/10.1103/PhysRevC.74.057602
22. C. Shen, Y. Abe, D. Boilley et al., Isospin dependence of reactions ^{48} Ca $+^{243-251}$Bk. Int. J. Mod. Phys. E **17**, 66 (2008). https://doi.org/10.1142/s0218301308011768
23. N. Wang, J. Tian, W. Scheid, Systematics of fusion probability in "hot" fusion reactions. Phys. Rev. C **84**, 061601 (2011). https://doi.org/10.1103/PhysRevC.84.061601
24. L. Zhu, Z.Q. Feng, C. Li et al., Orientation effects on evaporation residue cross sections in ^{48}Ca-induced hot fusion reactions. Phys. Rev. C **90**, 014612 (2014a). https://doi.org/10.1103/PhysRevC.90.014612
25. Z.Q. Feng, G.M. Jin, J.Q. Li et al., Formation of superheavy nuclei in cold fusion reactions. Phys. Rev. C **76**, 044606 (2007). https://doi.org/10.1103/PhysRevC.76.044606
26. L. Zhu, W.J. Xie, F.S. Zhang, Production cross sections of superheavy elements Z=119 and 120 in hot fusion reactions. Phys. Rev. C **89**, 024615 (2014b). https://doi.org/10.1103/physrevc.89.024615
27. L. Zhu, J. Su, F.S. Zhang, Influence of the neutron numbers of projectile and target on the evaporation residue cross sections in hot fusion reactions. Phys. Rev. C **93**, 064610 (2016). https://doi.org/10.1103/physrevc.93.064610
28. Z.H. Wu, L. Zhu, F. Li, X.B. Yu, J. Su, C.C. Guo, Synthesis of neutron-rich superheavy nuclei with radioactive beams within the dinuclear system model. Phys. Rev. C **97**, 064609 (2018). https://doi.org/10.1103/PhysRevC.97.064609
29. N.V. Antonenko, E.A. Cherepanov, A.K. Nasirov et al., Competition between complete fusion and quasi-fission in reactions between massive nuclei. Fus. Barrier. Phys. Lett. B **319**, 425 (1993). https://doi.org/10.1016/0370-2693(93)91746-a
30. G.G. Adamian, N.V. Antonenko, S.P. Ivanova et al., Problems in description of fusion of heavy nuclei in the two-center shell model approach. Nucl. Phys. A **646**, 29 (1999). https://doi.org/10.1016/s0375-9474(98)00616-2
31. G. Giardina, S. Hofmann, A.I. Muminov et al., Effect of the entrance channel on the synthesis of superheavy elements. Eur. Phys. J. A **8**, 205 (2000). https://doi.org/10.1007/s10050-000-4509-7
32. A.S. Zubov, G.G. Adamian, N.V. Antonenko et al., Competition between evaporation channels in neutron-deficient nuclei. Phys. Rev. C **68**, 014616 (2003). https://doi.org/10.1103/PhysRevC.68.014616
33. G.G. Adamian, N.V. Antonenko, W. Scheid et al., Possibilities of production of neutron-deficient isotopes of U, Np, Pu, Am, Cm, and Cf in complete fusion reactions. Phys. Rev. C **78**, 044605 (2008). https://doi.org/10.1103/PhysRevC.78.044605
34. J. Hong, G.G. Adamian, N.V. Antonenko, Possibilities of production of transfermium nuclei in charged-particle evaporation channels. Phys. Rev. C **94**, 044606 (2016). https://doi.org/10.1103/PhysRevC.94.044606
35. Z.Q. Feng, G.M. Jin, F. Fu et al., Production cross sections of superheavy nuclei based on dinuclear system model. Nucl. Phys. A **771**, 50 (2006). https://doi.org/10.1016/j.nuclphysa.2006.03.002
36. X.J. Bao, Y. Gao, J.Q. Li et al., Influence of nuclear basic data on the calculation of production cross sections of superheavy nuclei. Phys. Rev. C **92**, 014601 (2015b). https://doi.org/10.1103/PhysRevC.92.014601
37. K.H. Schmidt, W. Morawek, The conditions for the synthesis of heavy nuclei. Rep. Prog. Phys. **54**, 949 (1991). https://doi.org/10.1088/0034-4885/54/7/002
38. A.S. Iljinov, M.V. Mebel, N. Bianchi et al., Phenomenological statistical analysis of level densities, decay widths and lifetimes

of excited nuclei. Nucl. Phys. A **543**, 517 (1992). https://doi.org/10.1016/0375-9474(92)90278-r
39. A.S. Zubov, G.G. Adamian, N.V. Antonenko et al., Survival probability of superheavy nuclei. Phys. Rev. C **65**, 024308 (2002). https://doi.org/10.1103/PhysRevC.65.024308
40. P. Moller, J.R. Nix, W.D. Myers, Nuclear ground-state masses and deformations. At. Data Nucl. Data Tables **59**, 185 (1995). https://doi.org/10.1006/adnd.1995.1002
41. V. Weisskopf, Statistics and Nuclear Reactions. Phys. Rev. **52**, 295 (1937). https://doi.org/10.1103/physrev.52.295
42. M. Blann, Decay of deformed and superdeformed nuclei formed in heavy ion reactions. Phys. Rev. C **21**, 1770 (1980). https://doi.org/10.1103/physrevc.21.1770
43. N. Bohr, J.A. Wheeler, The Mechanism of Nuclear Fission. Phys. Rev. **56**, 426 (1939). https://doi.org/10.1103/physrev.56.426
44. R. Graeger, D. Ackermann, M. Chelnokov et al., Experimental study of the $^{238}\mathrm{U}\,(^{36}\mathrm{S}, 3-5n)^{269-271}\mathrm{Hs}$ reaction leading to the observation of ^{270}Hs. Phys. Rev. C **81**, 061601 (2010). https://doi.org/10.1103/PhysRevC.81.061601
45. Y.T. Oganessian, V.K. Utyonkov, F.S. Abdullin et al., Synthesis and study of decay properties of the doubly magic nucleus ^{270}Hs in the $^{226}\mathrm{Ra} + {}^{48}\mathrm{Ca}$ reaction. Phys. Rev. C **87**, 034605 (2013b). https://doi.org/10.1103/PhysRevC.87.034605
46. J. Dvorak, W. Brüchle, M. Chelnokov et al., Observation of the $3n$ evaporation channel in the complete hot-fusion reaction $^{26}\mathrm{Mg}+{}^{248}\mathrm{Cm}$ leading to the new superheavy nuclide ^{271}Hs. Phys. Rev. Lett. **100**, 132503 (2008). https://doi.org/10.1103/PhysRevLett.100.132503